CHARACTERIZING THERMOMECHANICAL PROPERTIES OF LARGE-FORMAT PRINTED COMPOSITE POLYMER STRUCTURES

Tyler Corum[1], Johnna O'Connell[1], Maximilian Heres[2], Jeff Foote[2], Chad Duty[1,3]

1.) Mechanical, Aerospace, and Biomedical Engineering Department at the University of Tennessee, Knoxville, TN 37996
2.) Loci Robotics, Inc., Knoxville, TN 37902
3.) Manufacturing Science Division at Oak Ridge National Laboratory, Oak Ridge TN 37830

Abstract

Large-format additive manufacturing (LFAM) is a manufacturing technique where a high volume of material is extruded in a layer-by-layer fashion to form structures that typically measure several meters in scale. The LOCI-One system is an LFAM-type system operated by Loci Robotics, Inc. that features a high throughput extruder mounted on a 6-axis robot arm. This research used the LOCI-One system to print single bead walls of 20% by weight carbon fiber reinforced acrylonitrile butadiene styrene (CF-ABS) at various layer deposition methods, print speed, layer times, and bead widths. The coefficient of thermal expansion (CTE) of the printed structures was measured to quantify effects of print conditions on thermomechanical performance. The CTE of the LFAM printed walls was measured using a large-scale digital image correlation system to characterize the distortion of the fiber reinforced composite material in the x- (print direction) and z- (between layers) directions. This study determined that with varying print parameters the CTE measured in the x-direction was largely influenced by bead geometry with the CTE measured in the z-direction relatively unaffected by either the varying parameters or the method in which layer deposition occurred.

Introduction

Additive manufacturing (AM) is an area of interest for industry because this manufacturing technique gives the ability to create complex geometries by only placing material where it is needed. Large-format AM (LFAM) allows large amounts of material (>1 m^3) to be deposited at fast rates (~50 kg/hr) [1–3]. Fiber reinforced polymer (FRP) is a common composite feedstock for these types of systems as it increases stiffness and reduces coefficient of thermal expansion (CTE) [1,4]. During extrusion, however, the reinforcing fibers shear align in the direction of the print, which results in a highly anisotropic LFAM bead with a highly aligned shell and randomly oriented bead core or center [5–8] as shown by Figure 1. The reinforcing fiber resists expansion differently with lower CTE exhibited in the longitudinal direction (parallel to direction of deposition, x-direction) than the transverse direction (perpendicular to direction of deposition, z-direction). With fibers oriented based on location within the bead and these same fibers providing directionally dependent resistance to expansion, the final LFAM structure has complex microstructure with highly anisotropic thermomechanical properties [9,10].

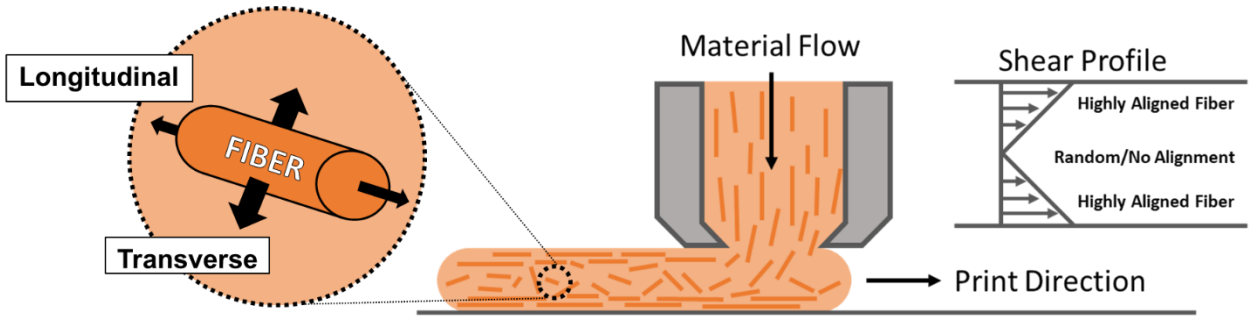

Figure 1. *Above shows the fiber alignment that occurs within an LFAM bead from nozzle shearing effects.*

Measuring CTE is traditionally done using methods such as thermomechanical analysis (TMA), but this fails to capture effects of the complex microstructure of an LFAM structure made using FRP [9–13]. TMA is a localized measurement technique that cannot accurately represent an LFAM structure both from sample dimension limitations and the small TMA sample must be representative of the entire part [9–11]. The method used in this study more accurately represents CTE by capturing global effects of the FRP microstructure by using 2D digital image correlation (DIC). This technique relies on speckling a face of interest and tracking position before and after thermal loading. Displacement vectors are then calculated and used to find the strain experienced by a sample face. This technique can capture large areas of interest and was used to better represent the LFAM structures in this work. A DIC Oven setup was used in this study with a schematic of major components shown by Figure 2 below. This method uses speckling to track thermal induced distortion before and after thermal loading via 2D-DIC. Other work lists the calibration and validation of the DIC technique as a method to better represent LFAM structures [10,11].

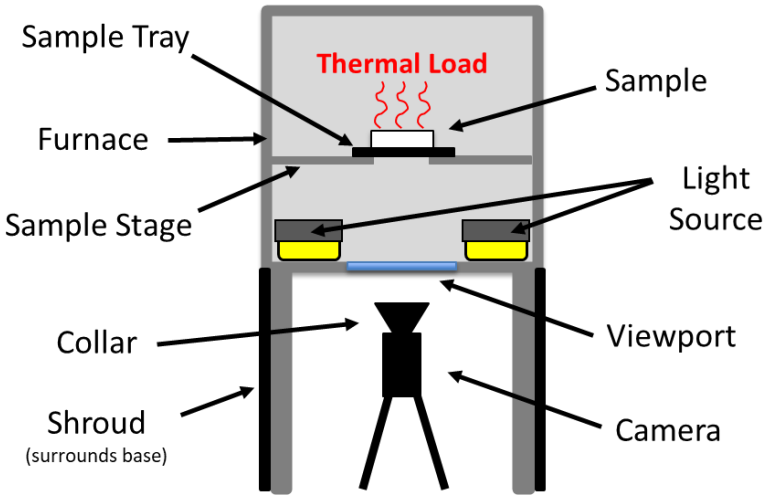

Figure 2. *A schematic of the DIC Oven with major components is shown.*

Methods and Materials

The FRP material used in this study was 20% by weight carbon fiber reinforced acrylonitrile butadiene styrene (CF-ABS). Loci Robotics Inc.'s LOCI-One system is an LFAM type system that utilizes a single screw extruder attached to the end of a KUKA 6-axis robot arm to achieve high precision and speed during printing. Single bead thick walls spanning only the x- and z-direction (XZ walls) were printed on the LOCI-One using different layer deposition methods and by varying parameters such as layer time, print speed, and bead width as shown by Table 1 below. The layer height was held constant at 5 mm for all samples. The layer deposition method used for each print was either a continuous layer deposition method (CLD) where the printer constantly printed each layer without interruption or the pause layer deposition method (PLD) where a dwell time was introduced to each layer to simulate a larger part being printed. To keep layer time consistent between "continuous" and "pause" printing, the print head velocity of the "pause" print was increased to accommodate a dwell period. The flow rate of each sample was calculated using equation 1 below where flow rate was represented by Q and was calculated from the print velocity (v), bead width (w), and layer height (h). This value increased with higher print speeds as well as with a larger bead geometry. Once the XZ walls were printed, 2x2 inch samples were waterjet cut and machined. These small plaques were then dried and speckled using the technique in [11]. This sampling process of the XZ walls is shown by Figure 3.

$$Q = vwh \qquad \text{EQ. 1}$$

Table 1. *Print parameters for this study are displayed below. The S, M, and L represent the small, medium, and large bead geometries.*

	Print Parameters						
Layer Deposition Method	Sample	Specimen	Bead Width (mm)	Layer Time (sec)	Dwell Time (sec)	Print Speed (mm/s)	Flow Rate (mm^3/s)
Continuous	1	1S	7.46	60	0	20	746
		1M	10.86	60	0	20	1086
		1L	14.16	60	0	20	1416
	2	2S	7.50	120	0	10	375
		2M	12.13	120	0	10	607
		2L	14.44	120	0	10	722
	3	3M1*	10.00	240	0	5	250
		3M2*	9.92	240	0	5	248
		3L	14.66	240	0	5	367
Pasue	4	4S	7.06	60	48	100	3530
		4M	10.32	60	48	100	5162
		4L	13.76	60	48	100	6882
	5	5S	7.16	120	108	100	3578
		5M	10.45	120	108	100	5225
		5L	13.50	120	108	100	6750
	6	6S	7.24	240	228	100	3620
		6M	10.41	240	228	100	5203
		6L	13.39	240	228	100	6697

** Note that the bead width for sample 3 have two similar widths that resemble values more like a medium size mead rather than a clear small and medium bead width*

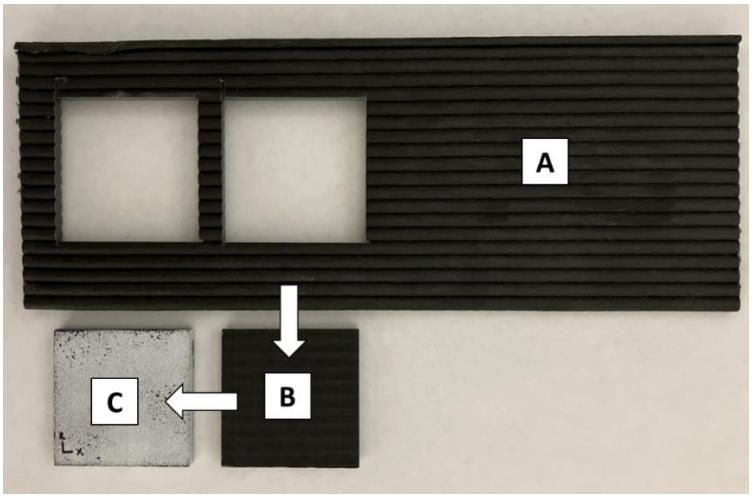

Figure 3. *The printed XZ wall is shown by A, the machined DIC plaque is shown by B, and the speckled DIC Oven sample is shown by C.*

The CTE of the plaques was then measured using the DIC Oven technique to measure average strain across a known thermal load. This process began by warming up the camera, positioning the sample, and adjusting the lighting as described in [11]. The sample was then imaged at room temperature using a camera with the room temperature state represented by a 45 image set taken in 100 ms intervals. The furnace was then set to 90 °C and the sample was allowed to reach thermal equilibrium. Once steady state was achieved based on the thermocouple study performed in [10], the steady state images were taken in 100 ms intervals for a total of 45 images to represent steady state. The sample was then rotated 90 degrees and re-measured to alleviate biasing from the lighting or positioning as described in [11]. The 90 total images were uploaded to Vic-2D where the average strain was calculated for each of the LFAM printed DIC plaques. With the known strain and temperature change, the CTE was calculated for each sample as in [10,11]. The average CTE of each sample was plotted ± 1 standard deviation.

Results

The Vic-2D software was used to create a strain contour map of each sample as shown by Figure 4. The figure on the left shows a relatively homogeneous, low magnitude strain in the x-direction (strain measured in the horizontal direction) while the figure on the right shows discrete bands of high strain in the z-direction (strain measured in the vertical direction). This behavior followed the expected trend based on fiber alignment. The CTE in the x-direction was much lower because this is the dominant direction of fiber alignment during extrusion, and the carbon fibers have a very low CTE along their axis. The z-direction shows red bands of high strain separating larger green bands of lower strain. The bands of high strain correspond to a higher concentration of fibers aligned in the x-direction that resist expansion poorly in the transverse (z) direction. The red areas correspond directly to the position of layer interfaces occur in the sample, where the most highly aligned fibers in the x-direction occur. The green, lower strain regions represent the more randomly oriented fiber at the center of each bead where a greater percentage of fibers are randomly aligned and thus provide greater resistance to thermal expansion in the z-direction.

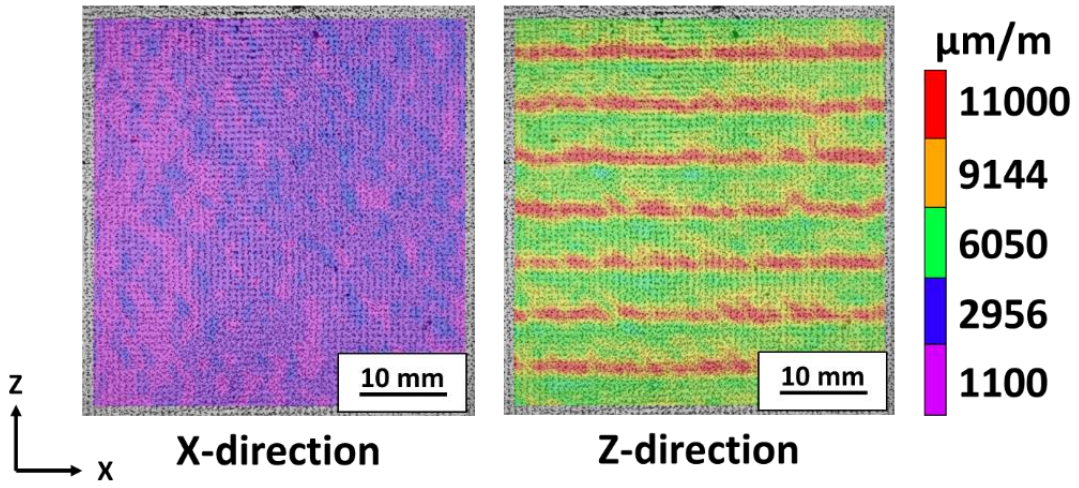

Figure 4. *The strain contour plot of sample 1S is shown here for the x and z-direction.*

The effects of aligned fibers are evident also in the Table 2 data which shows average CTE ± 1 standard deviation. Again, the x-direction CTE (CTE_x) is an order of magnitude lower than in the z-direction CTE (CTE_z) in each case regardless of print parameters. This CTE data is similar to data collected from thermomechanical properties of CF-ABS in [5,7].

Table 2. *Below shows average CTE data ± 1 standard deviation with the corresponding flow rates for each sample.*

CTE Values Measured by DIC Oven					
Layer Deposition Method	Sample	Specimen	CTE_x (μm/m°C)	CTE_z (μm/m°C)	Flow Rate (mm^3/s)
Continuous	1	1S	10.0 ± 0.8	123.6 ± 6.6	746
		1M	27.2 ± 1.3	126.0 ± 10.5	1086
		1L	29.3 ± 0.4	124.9 ± 4.6	1416
	2	2S	13.1 ± 1.9	124.8 ± 4.5	375
		2M	28.7 ± 1.5	127.1 ± 5.2	607
		2L	27.5 ± 0.6	124.9 ± 5.1	722
	3	3M1*	22.5 ± 2.6	127.7 ± 8.1	250
		3M2*	22.3 ± 1.6	117.9 ± 3.2	248
		3L	27.8 ± 0.9	123.2 ± 4.7	367
Pasue	4	4S	10.2 ± 1.5	123.1 ± 5.2	3530
		4M	23.7 ± 2.4	123.3 ± 4.4	5162
		4L	29.9 ± 2.3	123.5 ± 6.3	6882
	5	5S	12.4 ± 1.0	125.9 ± 5.9	3578
		5M	23.1 ± 1.5	117.1 ± 6.3	5225
		5L	28.6 ± 3.2	119.2 ± 5.1	6750
	6	6S	12.2 ± 2.1	123.5 ± 4.9	3620
		6M	24.1 ± 2.2	114.6 ± 7.7	5203
		6L	26.5 ± 1.2	118.3 ± 6.5	6697

The CTE of each sample with respect to flow rate in each direction is shown by Figure 5. This was done to best compare effects of the varying print parameters on the CTE of each sample. Comparisons of the different layer deposition methods used in the study were made by comparing sample sets 1 to 4, 2 to 5, and 3 to 6. The plot in Figure 5A shows that CTE_x decreases for the small bead geometry as the flow rate increases. This indicated that with increased material flow, more fibers were aligned in the x-direction and CTE_x values decreased as a result. The large and medium bead geometries did not show this same trend because the larger beads had a bigger core with randomly oriented fibers. Also, the wider beads experienced more flow normal to the bead axis as the extruded material beneath the deposition head was "squished outward". Figure 5C shows a trend of grouped data where the overall trend of the CTE_x values increases from small to medium to large. The PLD data is grouped with respect to flow rate because print speed was held constant during PLD prints with the data plotted based on similar bead geometry. With respect to CTE axis, the groups indicate that CTE_x values were not affected by the changing dwell times within each group of data points. For instance, with the small geometry of Figure 5C, the dwell

times increased from 48 seconds to 108 seconds to 228 seconds with relatively no change in CTE_x. The trend of increasing CTE_x values again is driven by bead geometry and is attributed to ratio of the highly aligned bead shell to the randomly oriented centers. As the bead geometry became larger, the region of randomly oriented fiber at the center of a bead became larger while the highly aligned shell region remained relatively constant. The plot in Figure 5B plot shows that the CTE_z values were relatively unaffected by the increasing flow rate. This makes sense as with the increased material flow, the layer height was constant, and did not change the amount of randomly oriented fibers relative to the highly aligned region. This trend is also seen by the Figure 5D plot that sees no relative change in the CTE_z values as material flow rate increased regardless of the dwell time introduced with each bead geometry.

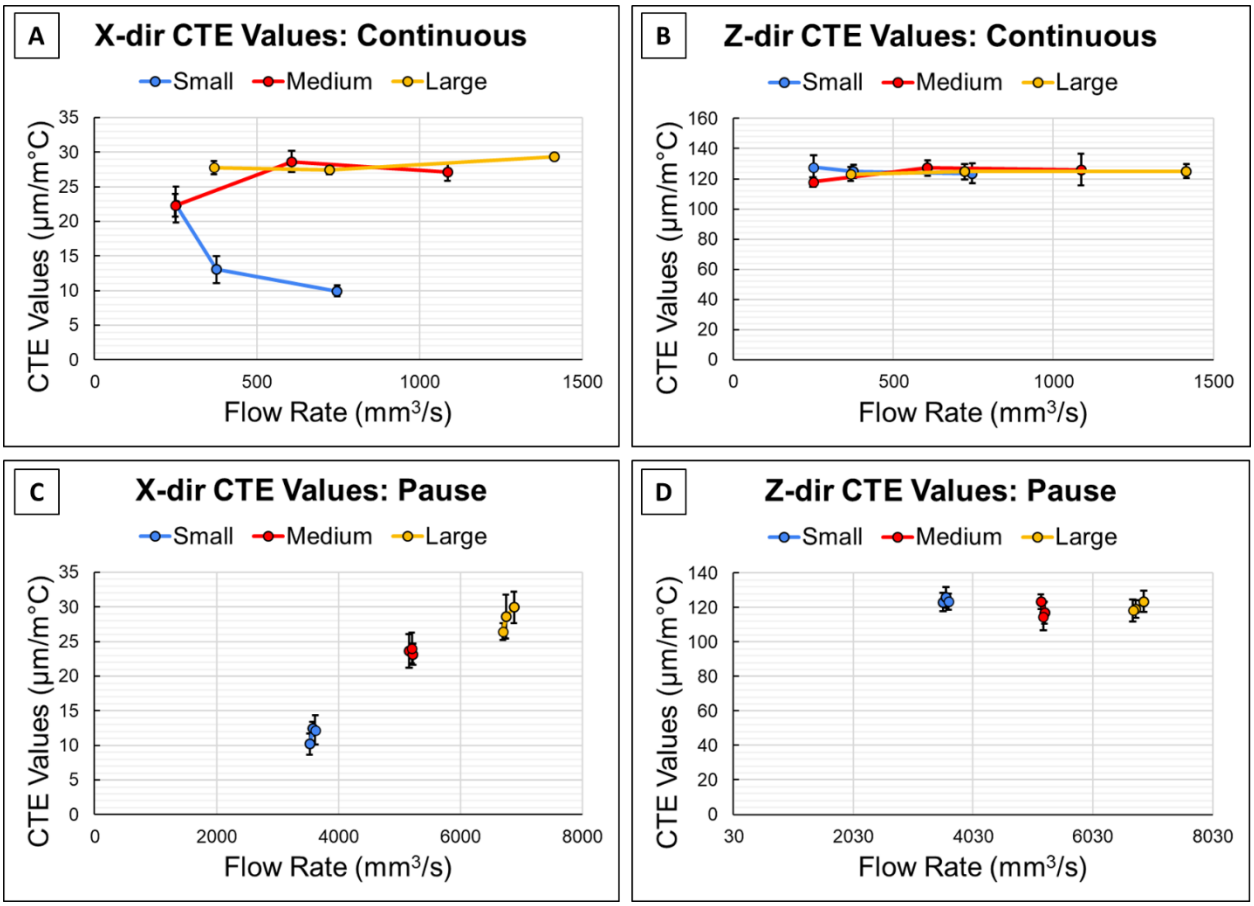

Figure 5. *The x-direction CTE is compared for both the CLD (A) and PLD (B) as well as z-direction CTE for both the CLD (C) and PLD (D).*

Conclusions

The aim of this study was to better characterize the thermomechanical properties of LFAM structures made using varying print parameters by using the DIC Oven to measure CTE. The strain plots presented in this work showed clear evidence of fiber alignment in the LFAM structures made of CF-ABS material printed using the LOCI-One system. Results showed that bead geometry was a dominant factor in the CTE values measured in the x-direction independent of the printing

method (CLD vs PLD). As bead geometry increased, CTE in the x-direction decreased due to the larger amounts of randomly oriented fiber at the bead center relative to the highly aligned shell. The CTE values in the z-direction, however, were relatively unaffected by either the increasing flow rate or the introduced dwell times from the PLD. This effect was due to the constant layer height of each LFAM structure not changing the relative percentage of the cross section regions containing aligned or randomly oriented fiber. Future work will be performed to relate the mechanical properties of these samples to varying print conditions as well as investigation thermal effects on layer bonding.

Acknowledgements

Special thanks to the Southeastern Advanced Machine Tools Network (SEAMTN) at the University of Tennessee, Knoxville for funding this research. Machining of samples was performed by the MABE Maker lab at the University of Tennessee. This research was sponsored by the U.S. Department of Energy, Office of Energy Efficiency and Renewable Energy, Advanced Manufacturing Office, under contract DE-AC05-00OR22725 with UT-Battelle, LLC.

References

[1] C.E. Duty, T. Drye, A. Franc, Material Development for Tooling Applications Using Big Area Additive Manufacturing (BAAM), 2015. https://doi.org/10.2172/1209207.
[2] C.E. Duty, V. Kunc, B. Compton, B. Post, D. Erdman, R. Smith, R. Lind, P. Lloyd, L. Love, Structure and mechanical behavior of Big Area Additive Manufacturing (BAAM) materials, Rapid Prototyp. J. 23 (2017) 181–189. https://doi.org/10.1108/RPJ-12-2015-0183.
[3] C. Duty, C. Ajinjeru, V. Kishore, B. Compton, N. Hmeidat, X. Chen, P. Liu, A.A. Hassen, J. Lindahl, V. Kunc, What makes a material printable? A viscoelastic model for extrusion-based 3D printing of polymers, J. Manuf. Process. 35 (2018) 526–537. https://doi.org/10.1016/j.jmapro.2018.08.008.
[4] L.J. Love, V. Kunc, O. Rios, C.E. Duty, A.M. Elliott, B.K. Post, R.J. Smith, C.A. Blue, The importance of carbon fiber to polymer additive manufacturing, J. Mater. Res. 29 (2014) 1893–1898. https://doi.org/10.1557/jmr.2014.212.
[5] K.M.M. Billah, F.A.R. Lorenzana, N.L. Martinez, R.B. Wicker, D. Espalin, Thermomechanical characterization of short carbon fiber and short glass fiber-reinforced ABS used in large format additive manufacturing, Addit. Manuf. 35 (2020) 101299. https://doi.org/10.1016/j.addma.2020.101299.
[6] A.A. Hassen, R.B. Dinwiddie, S. Kim, H.L. Tekinap, V. Kumar, J. Lindahl, P. Yeole, C. Duty, U. Vaidya, H. Wang, V. Kunc, Anisotropic thermal behavior of extrusion-based large scale additively manufactured carbon-fiber reinforced thermoplastic structures, Polym. Compos. 43 (2022) 3678–3690. https://doi.org/10.1002/pc.26645.
[7] J.L. Colón Quintana, L. Slattery, J. Pinkham, J. Keaton, R.A. Lopez-Anido, K. Sharp, Effects of Fiber Orientation on the Coefficient of Thermal Expansion of Fiber-Filled Polymer Systems in Large Format Polymer Extrusion-Based Additive Manufacturing, Materials. 15 (2022) 2764. https://doi.org/10.3390/ma15082764.
[8] P. Pibulchinda, E. Barocio, A.J. Favaloro, R.B. Pipes, Influence of printing conditions on the extrudate shape and fiber orientation in extrusion deposition additive manufacturing, Compos. Part B Eng. 261 (2023) 110793. https://doi.org/10.1016/j.compositesb.2023.110793.

[9] D. Hoskins, V. Kunc, A. Hassen, J. Lindahl, C. Duty, Characterizing Thermal Expansion of Large-scale 3D Printed Parts, in: SAMPE 2019 - Charlotte NC, SAMPE, 2019. https://doi.org/10.33599/nasampe/s.19.1598.
[10] T.M. Corum, J.C. O'Connell, A.A. Hassen, C.E. Duty, Measuring Thermally-Induced Distortion of Large-Scale Composite Printed Structures Using Digital Image Correlation, in: SAMPE Conf. Proc., Society for the Advancement of Material and Process Engineering - North America, Seattle, WA, 2023: p. 15. https://doi.org/10.33599/nasampe/s.23.0098.
[11] T. Corum, J. O'Connell, J. Brackett, R. Spencer, A. Hassen, C. Duty, Characterizing the Thermal-Induced Distortion of Large-Scale Polymer Composite Printed Structures, in: Proc. 33rd Annu. Int. SOLID Free. Fabr. Symp. 2022 – Addit. Manuf. Conf., Austin, TX, 2022: p. 20. http://dx.doi.org/10.26153/tsw/44338.
[12] A. Hassen, A. Lambert, J. Lindahl, D. Hoskins, C. Duty, S. Simunovic, C. Chin, V. Oancea, L. Love, Simulation Assisted Design for an Additively Manufactured Autoclave Tool Accounting for an Anisotropic Expansion, in: CAMX 2019, NA SAMPE, 2019. https://doi.org/10.33599/nasampe/c.19.0858.
[13] Z. Wang, A numerical study on the predicted fiber orientation of large area extrusion deposition additive manufactured composites, Polym. Compos. n/a (n.d.). https://doi.org/10.1002/pc.26731.